



Compositional complexity of heterogeneous impact glasses in lunar soils: significance and pitfalls

Qian W. L. Zhang¹ · Bin Su^{1,2} · Pierre Lanari³ · Jia-Hui Liu¹ · Jia-Long Hao⁴ · Yu Liu¹ · Liu-Yang Chen^{1,2} · Di Zhang¹ · Jiang-Yan Yuan¹ · Juan Wang⁵ · Xian-Hua Li^{1,2} · Qiu-Li Li^{1,2}

Received: 23 December 2024 / Accepted: 4 April 2025
© The Author(s) 2025

Abstract

Heterogeneous impact glass beads are abundant in lunar soils and have been extensively used to study the geological processes that shaped the Moon's surface. In this study, we examine the compositional complexity of three heterogeneous glass beads containing undigested zirconolite and zircon, using EPMA, Nano-SIMS mapping, and SIMS U–Pb isotope analyses. The undigested zircon and zirconolite crystals document three key volcanic events in the lunar history: at ~4.31 Ga the formation of alkali-suite rocks from the highlands, and at ~3.92 Ga, and ~2.04 Ga mare basalts, indicating that the U–Pb system in these zirconium-bearing crystals remains undisturbed during the ultra-high-temperature, short-duration impact melting events. EPMA and Nano-SIMS mapping reveal significant compositional inhomogeneity in the glass matrices, which complicates accurate provenance determination based on in-situ analysis. Bulk composition calculated from quantitative maps, however, provides a more reliable reference for inferring the origins of these beads. The high proportions of common Pb in the heterogeneous glass matrices, originating from diffusion-controlled processes during partial melting of impact involved minerals, introduce substantial uncertainties in U–Pb dating, complicating the interpretation of impact event ages. These findings highlight the challenges of U–Pb dating in heterogeneous glass beads and provide new insights into the preservation of pristine age information in lunar impact materials.

Keywords Lunar impact glass beads · Undigested minerals · Geochronology · In-situ analysis

Communicated by Ralf Dohmen.

✉ Qiu-Li Li
liqiuli@mail.iggcas.ac.cn

- ¹ State Key Laboratory of Lithospheric and Environmental Coevolution, Institute of Geology and Geophysics, Chinese Academy of Sciences, Beijing 100029, China
- ² College of Earth and Planetary Sciences, University of Chinese Academy of Sciences, Beijing 100049, China
- ³ Institute of Earth Sciences, University of Lausanne, Géopolis, CH-1015 Lausanne, Switzerland
- ⁴ Key Laboratory of Earth and Planetary Physics, Institute of Geology and Geophysics, Chinese Academy of Sciences, Beijing 10029, China
- ⁵ School of Resources and Environmental Engineering, Hefei University of Technology, Hefei 230009, China

Introduction

Impact glass beads are significant components of lunar soils (Li et al. 2022; Simon et al. 1981). They are formed by the rapid quenching of molten droplets generated during energetic meteoroid impacts on the lunar surface (Zellner 2019). As such, impact glass beads preserve valuable information about the external forces that have influenced the Moon. Previous studies have used lunar impact glass beads to explore the impact history of the Earth–Moon system through ⁴⁰Ar/³⁹Ar dating (Culler et al. 2000; Delano et al. 2007; Levine et al. 2005) and U-(Th)-Pb dating (Long et al. 2022; Nemchin et al. 2022; Norman et al. 2012, 2019), the average composition and evolution of local lunar regolith (Delano et al. 1981; Yang et al. 2022; Zellner 2019), and the lunar surface water budget (He et al. 2023; Liu et al. 2012; Zhou et al. 2024).

Since the impact melting and quenching of individual impact glass beads occur over very short timescales, typically less than one second (Arndt et al. 1984), the majority

(~70%) of these beads are heterogeneous (Chao et al. 1970; Chen et al. 2023; Norman et al. 2012). These beads contain undigested minerals or lithic clasts, indicating incomplete melting of the lunar regolith materials involved. Several in-situ microanalytical technologies, including electron probe microanalyzer (EPMA), secondary ion mass spectrometry (SIMS), nano-SIMS, and laser ablation inductively coupled plasma mass spectrometry (LA-ICP-MS), have been employed to analyse the major-, trace-element compositions, and radioisotope (uranium–lead/U–Pb) data of impact glass beads (Fig. 1) (Korotev et al. 2010; Long et al. 2022; Nemchin et al. 2022; Norman et al. 2019; Wang et al. 2024; Zhou et al. 2024). While homogeneous beads are ideal targets for in-situ analyses, many studies also include heterogeneous beads with sufficiently large glass patches for measurement. However, partially molten beads often exhibit complex textures and compositional zones, complicating the interpretation of in-situ analysis data. A recent U–Pb dating study of various Chang’e-5 impact glass beads revealed that the heterogeneous beads contain higher proportions of common

Pb (non-radiogenic Pb), resulting in systematically older calculated ages compared to the homogeneous group (Long et al. 2022). This systematic bias poses a potential challenge for the interpretation and accurate statistics of the growing database of impact glass beads. However, the mechanism by which undigested minerals influence the chemical composition of the glass matrix remains unclear.

In this study, we identified three impact glass beads containing undigested zirconium-bearing minerals (zirconolite and zircon) in the Chang’e-5 lunar soil samples. We performed element mapping using EPMA and Nano-SIMS and conducted U–Pb and Pb/Pb isotope analyses using SIMS for the three beads. Our data reveal the compositional complexity of the glass matrix in heterogeneous impact glasses. Tracing the provenance and dating the formation age of such heterogeneous glasses require careful consideration.

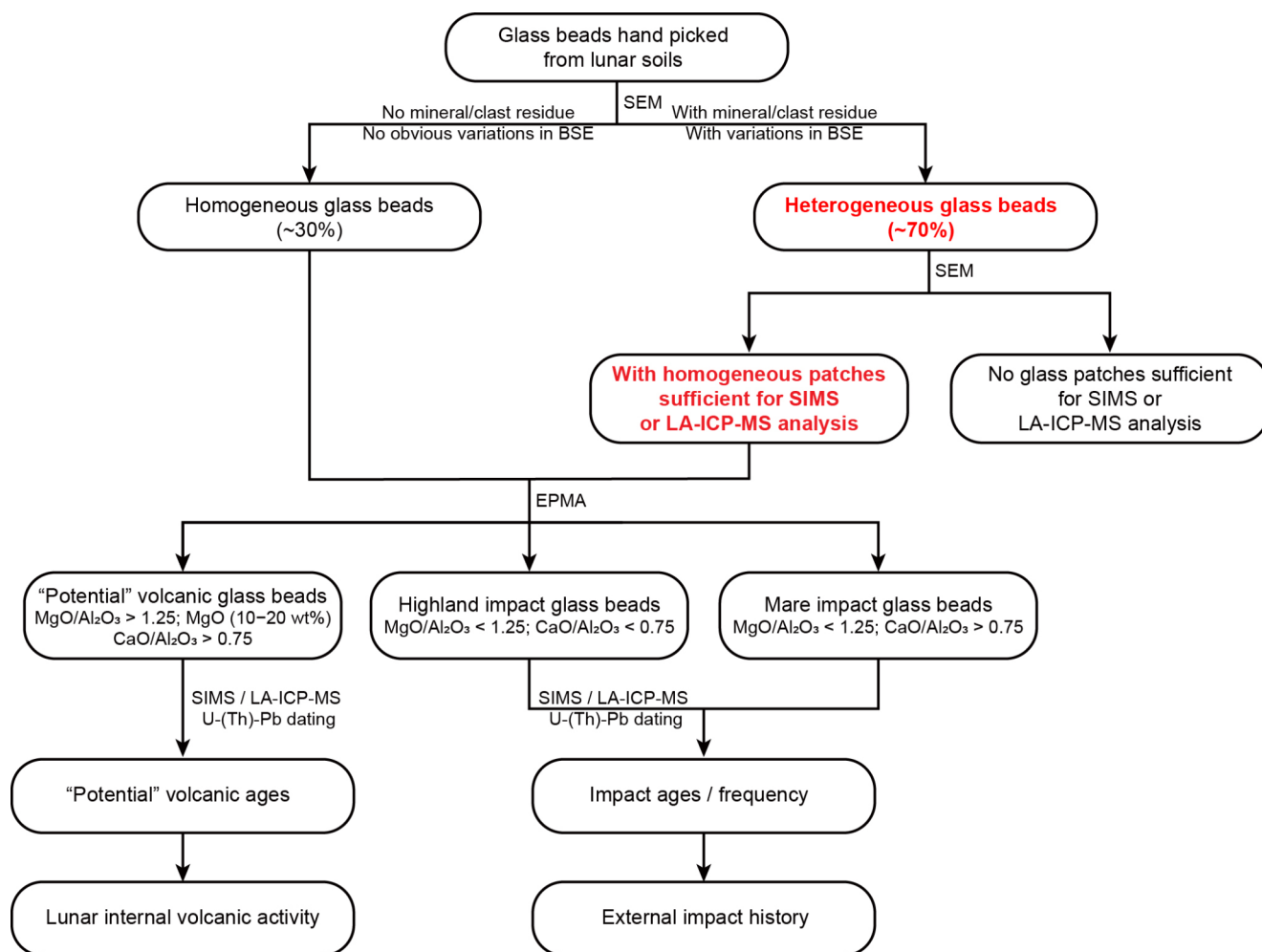


Fig. 1 General workflow of previous studies on glass beads in lunar soils specifically using in-situ analytical techniques. Note that some heterogeneous glass beads with sufficiently large homogeneous glass patches were also used for EPMA, SIMS, or LA-ICP-MS analyses

Materials and methods

Materials

Approximately 2000 glass beads were hand-picked from samples of the Chang'e-5 lunar soils (CE5C1000YJFM00301, 00403, 00404, and CE5Z0806YJFM006) allocated by the China National Space Administration. These glass beads were embedded in transparent epoxy mounts and polished for further analysis. The mounts were coated with a carbon layer for scanning electron microscope (SEM) and EPMA analyses, and with a gold layer for SIMS and nano-SIMS analyses.

SEM analysis

A Zeiss Gemini 450 field emission SEM equipped with an energy dispersive spectroscopy (EDS) detector at the Institute of Geology and Geophysics, Chinese Academy of Sciences (IGGCAS) in Beijing was used to acquire back-scattered electron (BSE) images and perform EDS analyses to identify the undigested mineral phases in heterogeneous beads. The acceleration voltage was set to be 15 kV with a current of 2.0 nA. Through this procedure, three impact glass beads containing zirconolite or zircon of sufficient size for SIMS analyses were identified. The compositions of tiny olivine inclusions were determined using EDS.

EPMA quantitative mapping

Major and minor element X-ray intensity maps of the three glass beads were obtained using a JEOL JXA-8230 electron probe micro-analyser (EPMA) at the School of Resources and Environmental Engineering, Hefei University of Technology, China. The analysis conditions were: an accelerating voltage of 15 keV and a specimen current of 100 nA. The mapping of glasses Nos. 1, 2, and 3 was carried out with pixel sizes of 0.24 μm , 0.28 μm , and 0.30 μm , respectively, and the same dwell time of 70 ms. Four round scans were conducted, with the first round covering elements Mg, S, Na, and P; the second round covering elements Al, K, Si, and Mn; the third round covering elements Ca and Fe, and the fourth round covering elements Ti and Zr. Spot analyses for major mineral phases and glasses were calibrated using SPI (Structure Probe Inc.) international standard samples, Smithsonian microbeam standards and GB/T 17359-1998 (Zhou Jianxiong standards group). Spot analytical data were used as internal standards for quantifying intensity maps. X-ray maps were corrected for dead time, classified, and standardized using XMapTools 4.3 (Lanari and Tedeschi 2025; Lanari et al. 2014, 2019). Structural formulae and

maps of end-member proportions were generated using the functions provided in XMapTools.

SIMS isotope analysis

The Pb isotope compositions of the zirconolite and host glass matrix in impact glass bead No. 1 (Supplementary Table S1), as well as the U–Pb isotope compositions of two zircon grains in glass beads Nos. 2 and 3 (Supplementary Table S2), were determined using a CAMECA IMS 1280HR ion microprobe at IGGCAS. The mount was cleaned with a fine (0.25 μm) diamond paste and ethanol to remove the carbon coating before adding a roughly 20-nm gold coating. A Gaussian illumination mode was used to focus a primary beam of $^{16}\text{O}^-$ to a size of $\sim 3 \mu\text{m}$, with an accelerated potential of -13KV and beam intensity of 200 pA.

For Pb isotope analysis, the multi-collector mode with five electron multipliers was used to measure $^{204}\text{Pb}^+$ (L2), $^{206}\text{Pb}^+$ (L1), $^{207}\text{Pb}^+$ (C), $^{208}\text{Pb}^+$ (H1), and $^{96}\text{Zr}_2^{16}\text{O}_2^+$ (H2). The methodology followed was similar to that outlined in Li et al. (2010). Exit slit 3 was used with a mass resolving power (MRP) of 8,000 (50% peak height). The ion images with $^{96}\text{Zr}_2^{16}\text{O}_2^+$ and Pb isotopes on a 25 $\mu\text{m} \times 25 \mu\text{m}$ area were used to precisely locate the target minerals. The signal of ^{206}Pb was used for peak-centring reference. Each spot measurement consisted of 4 s \times 80 cycles, with a total analytical time of about 10 min. NIST610 glass (Baker et al. 2004) and Phalaborwa baddeleyite standards (Heaman 2009) were used to calibrate the relative yield of different electron multipliers and evaluate the external reproducibility. Measured Pb isotopes were corrected for common Pb using non-radiogenic ^{204}Pb .

For U–Pb isotope analysis, the electron multiplier of the mono-collector system was used as the secondary ion beam detector. Each measurement consisted of 15 cycles, with a total analytical time of approximately 20 min. The U–Th–Pb isotope ratios were determined against the Plešovice zircon standard (Sláma et al. 2008). The Qinghu standard with reference age of $159.5 \pm 0.2 \text{Ma}$ (Li et al. 2013) was used as an unknown sample to monitor accuracy. A total of seven analyses of the Qinghu zircon yield a concordia age of $158.9 \pm 1.4 \text{Ma}$, which is identical to the reference value. Measured U–Pb isotopes were corrected for common Pb using non-radiogenic ^{204}Pb . Data reduction was carried out using the Excel add-in Isoplot package (Ludwig 2008). Individual uncertainties are reported at 1σ , and the weighted mean $^{207}\text{Pb}/^{206}\text{Pb}$ ages were calculated at a 95% confidence level. The detailed procedures followed those described in Li et al. (2010) and Liu et al. (2020).

Nano-SIMS element mapping

Enlarged maps (Fig. 8) of the zirconolite and its surrounding glass matrix were acquired using a CAMECA 50L Nano-SIMS at IGGCAS. A focused ~ 10 pA oxygen beam in the Gaussian mode with a beam size of ~ 250 nm in diameter was used. Seven secondary ion images, including ^{40}Ca , ^{48}Ti , ^{56}Fe , ^{89}Y , ^{94}Zr , and ^{208}Pb , were acquired by rastering a $25 \times 25 \mu\text{m}^2$ area with 512×512 pixels (single-pixel size 50 nm) and a dwell time of 785 s/frame. The total mapping time was ~ 4.6 h. The analyses followed the methods of Hao et al. (2016) and Hao et al. (2024). Recorded ion images were processed and analysed using ImageJ with Open MIMS plugin. Firstly, all frames of ion images for each element were automatically aligned using the TurboReg ImageJ plugin. Subsequently, these drift-corrected frames were combined. The denoising process followed the methods described by Hao et al. (2021). Due to the lack of reference materials to correct the matrix effect, only relative concentrations represented by counts per second (cps) are shown. Trace element cps data along a given profile in the ion images were extracted using XMapTools 4.3 (Lanari et al. 2014, 2019).

Results

Petrography and major element compositions

Based on numerous BSE images and EDS data, three glass beads containing undigested zirconolite and zircon crystals with grain sizes greater than $10 \mu\text{m}$ were identified from approximately 2000 glass beads in the allocated Chang'e-5 samples. These three beads exhibit similar petrographic features but varying proportions of mineral phases, along with abundant vesicles (Fig. 2). Glass bead No. 1 is predominantly composed of glass matrix (~ 65 vol%) and plagioclase ($\sim 28\%$), with minor amounts of zirconolite, ilmenite, olivine, clinopyroxene, apatite, Fe particles, and troilite (Fig. 2a). A triangular zirconolite crystal, approximately $30 \mu\text{m}$ in size, displays smooth edges and contains baddeleyite and ilmenite inclusions or intergrowths (Fig. 2b). Glass bead No. 2 primarily consists of glass matrix (~ 91 vol%), with subordinate plagioclase ($\sim 6\%$), zircon ($\sim 2\%$), and minor quartz, Fe particles, and troilite (Fig. 2c). A $10 \mu\text{m}$ zircon crystal is located at the edge of this glass bead, surrounded by numerous nanoscale zircon particles that increase in size with distance from the undigested zircon core (Fig. 2d). Glass bead No. 3 comprises glass matrix (~ 67 vol%), plagioclase ($\sim 25\%$), quartz (5%), and minor zircon, ilmenite, olivine, Fe particles, and troilite (Fig. 2e). The zircon crystal in this bead preserves rounded

with clearly defined edge, showing no evidence of melting or decomposition (Fig. 2f). Additionally, an Fe particle is encased by troilite that formed later.

The glass matrix within each bead shows noticeable compositional heterogeneity, as revealed by compositional mapping of major elements (Figs. 3, 4, 5). For example, the variations of MgO content in glass beads Nos. 1–3 are 4.5–7.5 wt%, 5.0–7.0 wt%, and 4.0–9.0 wt%, respectively. CaO contents range from 9.0 to 12.0 wt%, 9.5–11.0 wt%, and 10.0–14.0 wt%, respectively. Al_2O_3 contents vary from 10.0 to 25.0 wt%, 9.0–11.5 wt%, and 10.0–20.0 wt%, respectively. The compositional anomaly regions are closely associated with the spatial distribution of residual minerals. High- Al_2O_3 , high-MgO, and high-FeO regions are predominantly distributed along the edges of undigested plagioclase, olivine, and ilmenite, respectively (Figs. 3, 4, 5). In glass beads Nos. 2 and 3, the glass matrix surrounding undigested zircon crystals shows significantly elevated ZrO_2 concentrations (up to >6 wt%). Plagioclase is a common undigested mineral phase, and its X_{An} (anorthite content) values also exhibit significant heterogeneity, both between and within individual crystals in each bead (Fig. 6). The ranges of X_{An} of plagioclase in the three beads are 0.70–0.95 (No. 1), 0.83–0.89 (No. 2), and 0.75–0.95 (No. 3), reflecting the inheritance of compositions from pristine magmatic plagioclases.

Radioisotope dating of zirconolite and zircon crystals

SIMS Pb–Pb dating and U–Pb dating were performed on zirconolite and zircon crystals within the three impact glass beads, respectively. For the $\sim 30 \mu\text{m}$ triangular zirconolite within glass No. 1, eight Pb–Pb analyses were conducted using $\sim 3 \mu\text{m}$ spot size. The results show extremely low $^{204}\text{Pb}/^{206}\text{Pb}$ ratios ($<7 \times 10^{-7}$) (Supplementary Table S1), meaning the radiogenic ^{206}Pb accounts for more than 99.9% of the total ^{206}Pb and the common Pb (non-radiogenic Pb) correction has a negligible effect on the ages. The eight analyses yield consistent $^{207}\text{Pb}/^{206}\text{Pb}$ ages (Supplementary Table S1), with a weighted mean age of 4310 ± 13 Ma [2σ ; MSWD (mean square weighted deviation) = 1.5] (Fig. 7a). Three U–Pb spot analyses were performed on the residual zircon crystal within glass No. 2 (Supplementary Table S2). One spot, located in the undigested zircon core, yields concordant age with a $^{207}\text{Pb}/^{206}\text{Pb}$ age of 3921 ± 14 Ma showing a high U concentration of $\sim 94 \mu\text{g/g}$ (Supplementary Table S2). In contrast, the other two spot analyses, situated in regions enriched with nanoscale zircon particles, are discordant and exhibit low U concentrations of (Supplementary Table S2). For the zircon crystal in the glass No. 3, five SIMS U–Pb analyses (Supplementary Table S2) fall on or

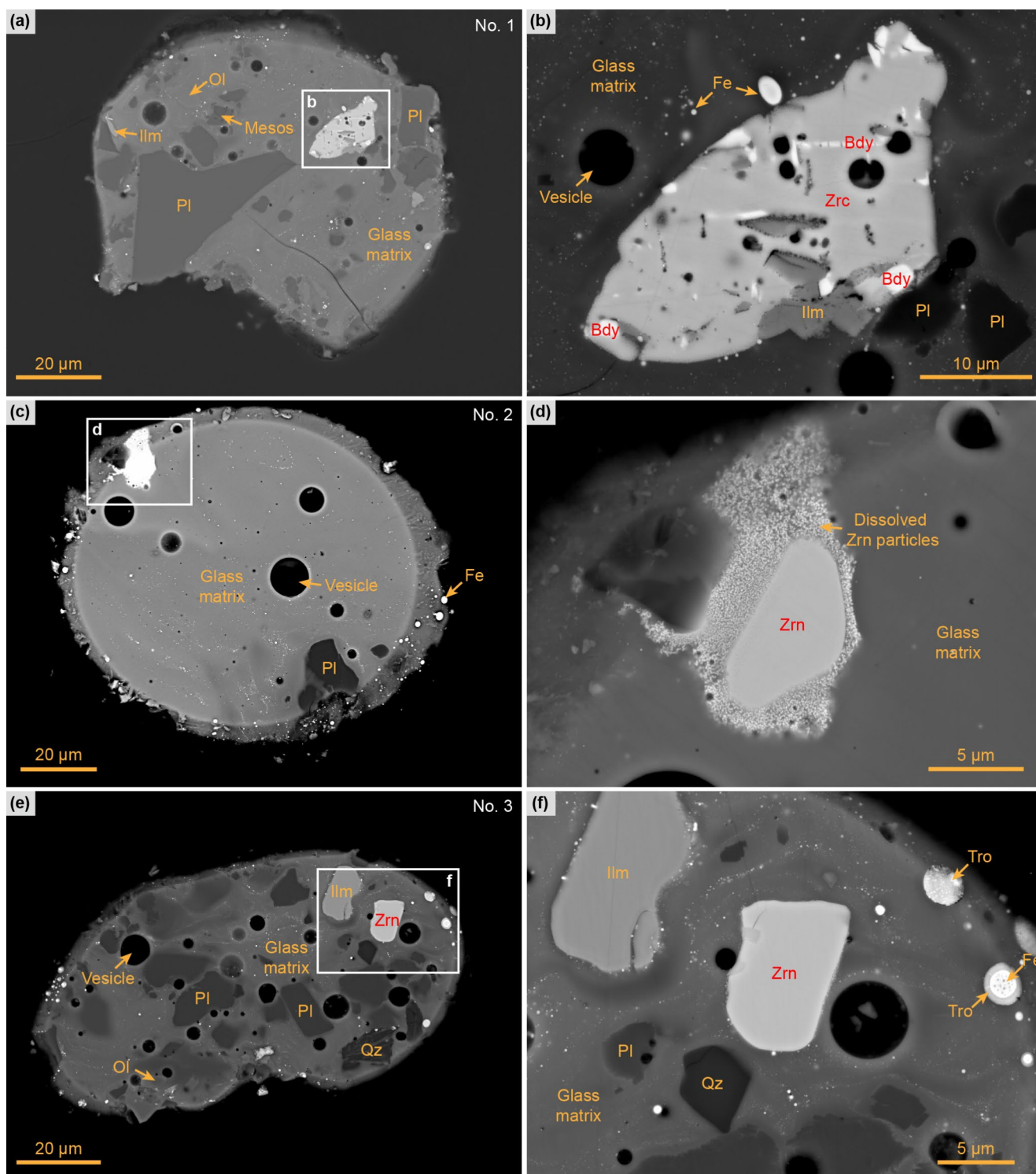


Fig. 2 BSE images of three impact glass beads containing zirconolite and zircon crystals. **a** BSE image of bead No. 1 displaying various undigested mineral facies. Mineral abbreviations follow Warr (2021). **b** Enlarged BSE image of the zirconolite crystal in **a**. Baddeleyite

occurs as tiny grains along the edges or as exsolution bands. **c** BSE image of bead No. 2. **d** Enlarged BSE image of the zircon crystal in **c** showing dissolved nanoscale particles. **e** BSE image of bead No. 3. **f** Enlarged BSE image of the zircon crystal in **e**

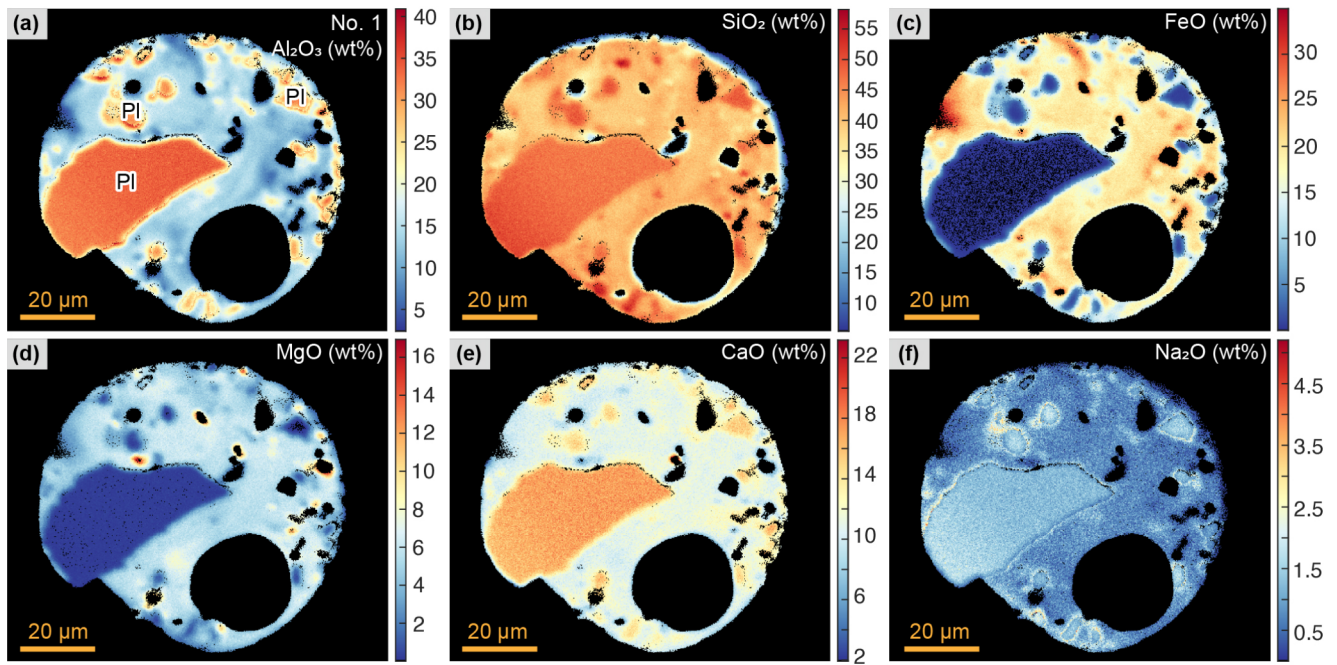


Fig. 3 Quantitative compositional mapping results of glass bead No. 1. **a–f** Elemental oxide maps (wt%) of Al_2O_3 , SiO_2 , FeO , MgO , CaO , and Na_2O , respectively, in glass bead No. 1. The discrepancy between BSE

images and EPMA maps is due to additional polishing of the sample surface after SIMS and NanoSIMS analyses

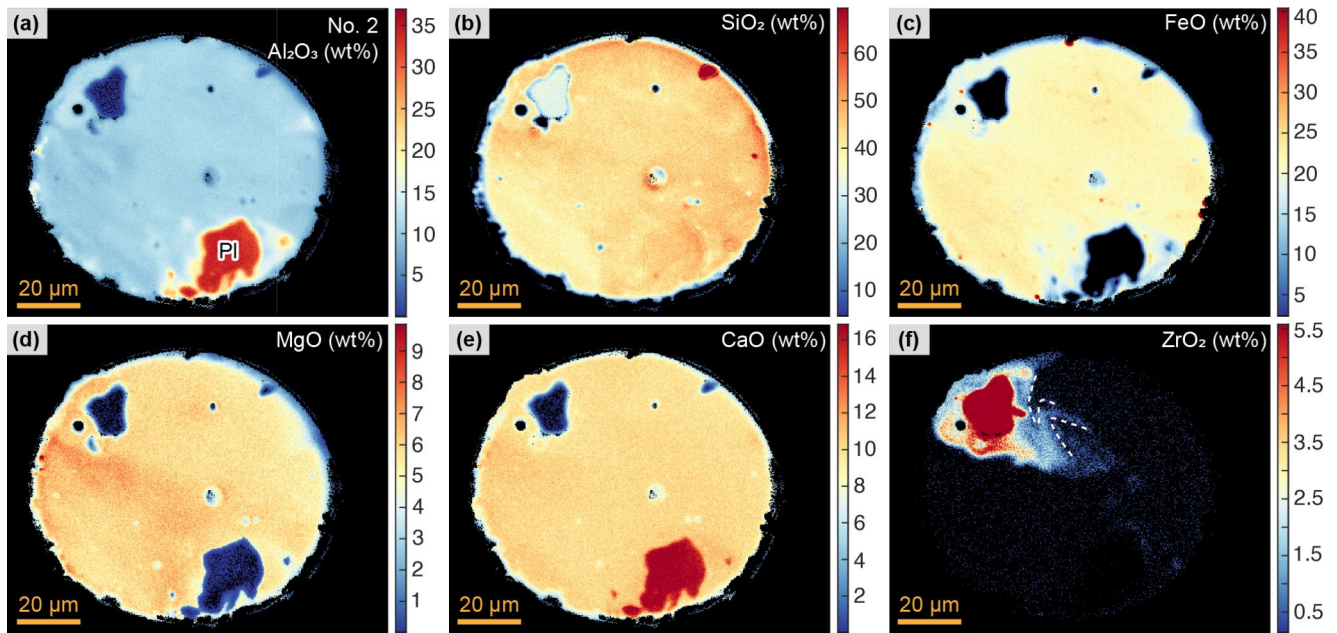


Fig. 4 Quantitative compositional mapping results of glass bead No. 2. **a–f** Elemental oxide maps (wt%) of Al_2O_3 , SiO_2 , FeO , MgO , CaO , and ZrO_2 , respectively, in glass bead No. 2. In **e** and **f**, the colour scale

limits were adjusted to emphasize chemical variations at low wt%; as a result, regions with higher wt% values exceeding the upper limit are displayed using the final colour of the bar

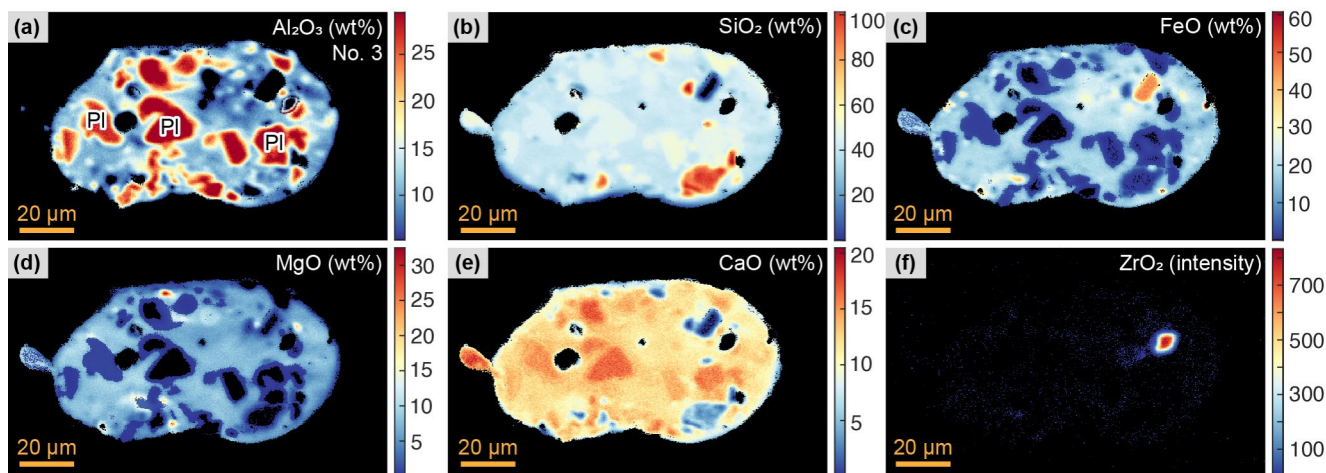


Fig. 5 Quantitative compositional mapping results of glass bead No. 3. **a–f** Elemental oxide maps (wt%) of Al_2O_3 , SiO_2 , FeO , MgO , CaO , and ZrO_2 , respectively, in glass bead No. 3

near the Concordia curve, which yields a weighted mean $^{207}\text{Pb}/^{206}\text{Pb}$ age of 2043 ± 53 Ma (MSWD=0.1; Fig. 7c).

Pb isotope and nano-SIMS mapping of glass matrix

SIMS Pb isotope spot analysis was conducted on the glass matrix in bead No. 1. Six, four, and three spot analyses were performed along three profiles (P1–P3; Fig. 8a), respectively. The count rate of ^{206}Pb for the spot closest to the zirconolite is as high as 1035 cps, while for spot farthest from the zirconolite is less than 10 cps (Supplementary Table S1). Along all three profiles, the ^{206}Pb cps values, representing relative ^{206}Pb abundances, show a trend of gradually decreasing with distance from the zirconolite (Fig. 8f–h). Compared to the ~ 4.31 Ga zirconolite, the $^{207}\text{Pb}/^{206}\text{Pb}$ ratios of the glass matrix exhibit larger uncertainties (Fig. 8i) due to lower Pb abundance and ion yield of secondary Pb ions in glasses. Although the spots on the glass matrix show significantly varying Pb abundances, their $^{207}\text{Pb}/^{206}\text{Pb}$ ratios are generally consistent with or slightly higher than those of the zirconolite (Fig. 8i).

The distributions of trace isotopes ^{208}Pb , ^{46}Ti , ^{89}Y , and ^{94}Zr in the glass matrix surrounding the zirconolite crystal were mapped using Nano-SIMS with a single-pixel size of ~ 50 nm (Fig. 8b–e). The production rate of secondary Pb ion in the glass matrix during Nano-SIMS analysis is very low, resulting in low cps values of ^{208}Pb (< 1). After denoising, the ^{208}Pb map reveals that Pb abundance in the glass near the zirconolite is slightly higher than in the glass farther away (Fig. 8b). The production rates of secondary Ti, Y, and Zr ions in the glass matrix are higher than that of Pb, with the highest cps values of Ti, Y, and Zr ions being 80, 14, and 6, respectively. The decreasing trends of the abundances of these elements away from the zirconolite are more pronounced than that of Pb, as shown by the maps (Fig. 8c–e)

and profiles of normalized cps values (Fig. 8j; Supplementary Table S3). Similar decreasing trends of Zr abundances are also observed in the maps obtained by EPMA mapping (Figs. 4f, 5f). Notably, some elements, such as Ti and Zr, exhibit complex, streamlined distributions (Figs. 4f, 8c and e).

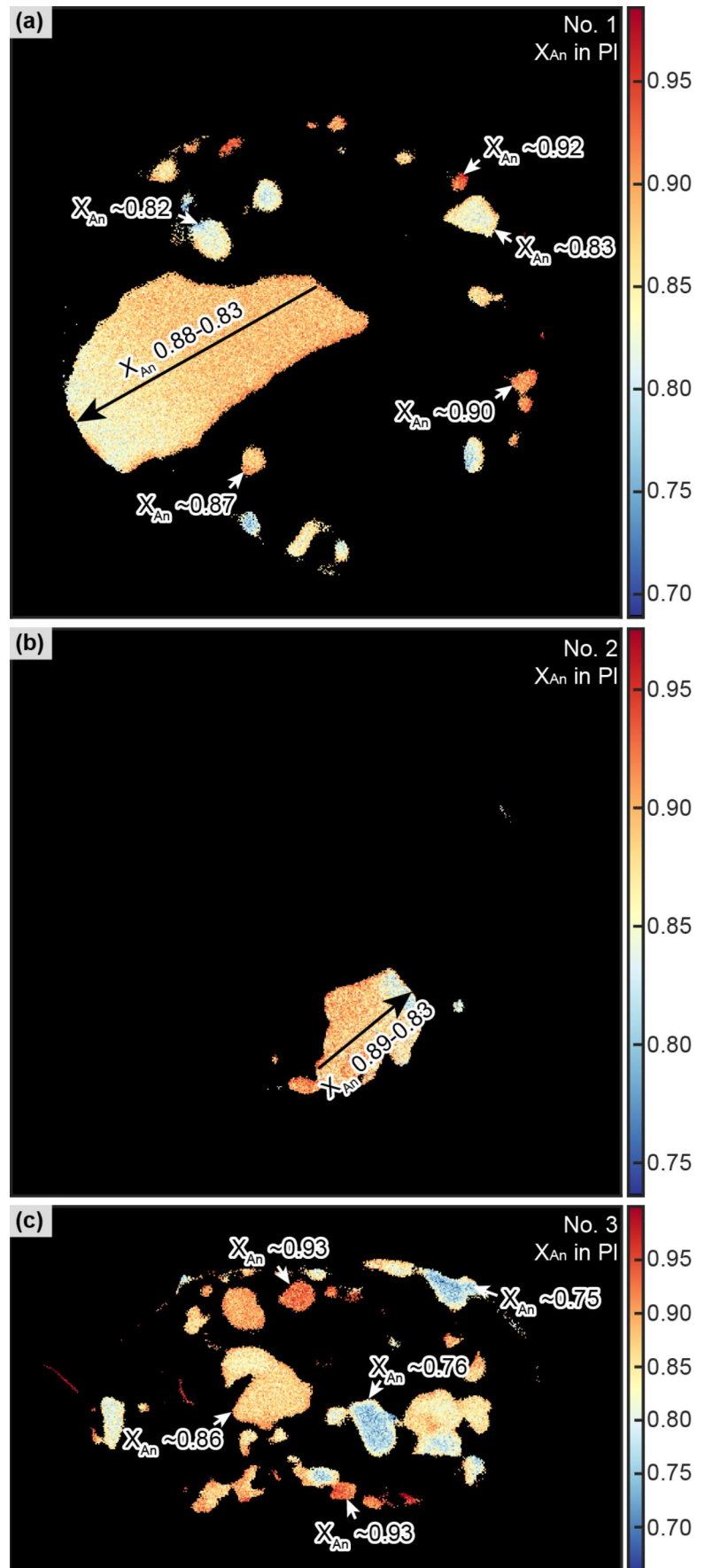
Discussion

Undisturbed U–Pb system in zirconolite and zircon in glass beads

Meteoroid impacts are major geological processes that modify the lunar surface (e.g., Adams et al. 1975; Morris 1978). Large-scale meteoroid impacts can induce varying degrees of melting of precursor lunar regolith materials (e.g., Bischoff and Stoffler 1992; Cintala and Grieve 1998; Delano 1991; Ryder and Spudis 1987). A significant number of zircon and zirconolite crystals, either inherited from precursor magmatic rocks, or recrystallized and newly formed within impact melts, have been identified in various impact-generated breccia fragments from Apollo samples. U–Pb dating of these zircon crystals provides important constraints on the early volcanic history of the Moon, spanning from 4.42 to 4.0 Ga (Nemchin et al. 2008, 2009, 2012), as well as on early impact events prior to 3.9 Ga (Barboni et al. 2024; Grange et al. 2009; Nemchin et al. 2012; Norman and Nemchin 2014).

Impact glass beads underwent a higher degree of partial melting compared to impact breccia. It remains uncertain whether undigested zirconium-bearing minerals can retain pristine age information from before the impact. This study presents the first identification and geochronological constraints on zircon and zirconolite as residual minerals in

Fig. 6 X_{An} (anorthite content) maps of undigested plagioclase crystals in the three heterogeneous glass beads Nos. 1–3



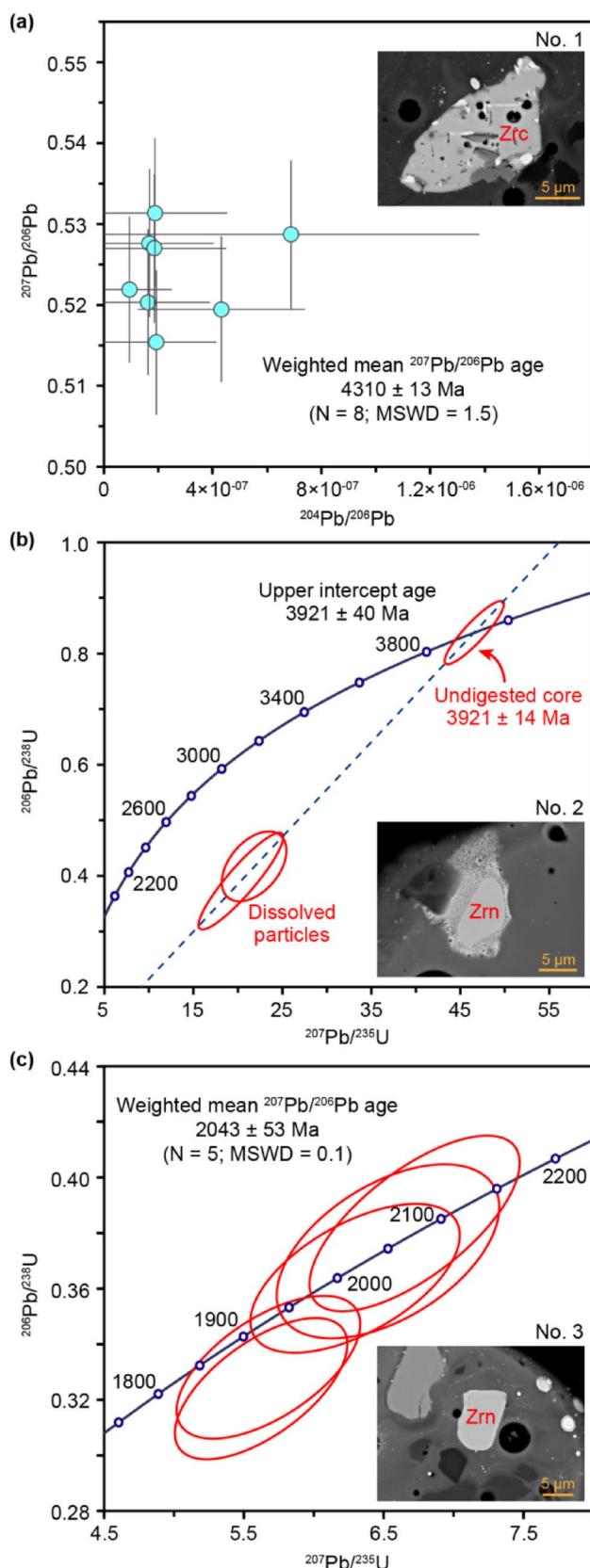


Fig. 7 Pb–Pb and U–Pb dating results of zirconolite and zircon crystals in three impact glass beads. **a** Pb–Pb dating results of the zirconolite crystal in glass No. (1) **b** U–Pb dating results of the zircon crystal in glass No. (2) **c** U–Pb dating results of the zircon crystal in glass No. 3

heterogeneous impact glass beads formed during impact-induced melting. For the zirconolite crystal in glass No. 1 (Fig. 2a, b), eight SIMS analyses with a spatial resolution of 3 μm show consistent $^{207}\text{Pb}/^{206}\text{Pb}$ ages of 4.31 Ga (Fig. 7a), indicating no significant Pb migration (loss or segregation) within the crystal during the impact event. Therefore, the average $^{207}\text{Pb}/^{206}\text{Pb}$ age of 4310 ± 13 Ma is interpreted as the formation age of pristine zirconolite. The zircon crystal in glass bead No. 2 exhibits an obvious dissolved structure, with a surviving core surrounded by numerous nanoscale zircon particles (Fig. 2c, d). SIMS U–Pb analyses reveal that the surviving core records a concordant age of 3921 ± 14 Ma, suggesting no significant loss of radiogenic Pb. In contrast, the other nanoscale zircon particles show discordant U–Pb ages (Fig. 7b), indicating partial loss of radiogenic Pb during the decomposition process induced by impact melting. The zircon crystal in bead No. 3 shows a rounded shape with clearly defined edge (Fig. 2e, f), suggesting minimal influence from partial melting. Consistent with this, the five U–Pb analyses yield consistent $^{207}\text{Pb}/^{206}\text{Pb}$ ages with a weighted mean value of 2043 ± 53 Ma (Fig. 7c).

These data indicate that zircon and zirconolite in impact glass beads can preserve pristine U–Pb age despite experiencing high-temperature impact melting. Conventional closure temperatures for the U–Pb system in zircon and zirconolite are estimated to be around 800–900 $^{\circ}\text{C}$ under typical geological cooling rates (Cherniak and Watson 2001; Wu et al. 2010). Such estimates are not applicable to the extreme conditions associated with lunar impact glass beads. During ballistic flight on the lunar surface, melt droplets cool at ultrafast rates on the order of ~ 1500 $^{\circ}\text{C}/\text{s}$ and 4200 $^{\circ}\text{C}/\text{s}$ for ~ 220 to ~ 94 μm beads (Arndt et al. 1984). To better account for such rapid cooling scenarios, we applied the diffusion parameters of Cherniak and Watson (2001) within the closure temperature calculation model of the Ganguly and Tirone (1999). The results suggest that under these high cooling rates, the closure temperature effectively approaches the peak temperature of the impact melt droplet (> 1200 $^{\circ}\text{C}$) (Manske et al. 2022), meaning the system likely never exceeded its closure temperature during cooling. As a result, the U–Pb system in undigested zircon and zirconolite remained effectively closed. This supports our interpretation that the measured U–Pb ages represent pristine crystallization ages, and not impact-reset ages.

Provenance of the three impact glass beads

The Chang'e-5 landing site is located in the Em4 mare basalt unit, northwest of the Ocean Procellarum (Li et al. 2022). Radioisotope dating reveals that various basaltic fragments in this region share a consistent formation age of 2030 ± 4 Ma (Li et al. 2021), indicating that the Chang'e-5

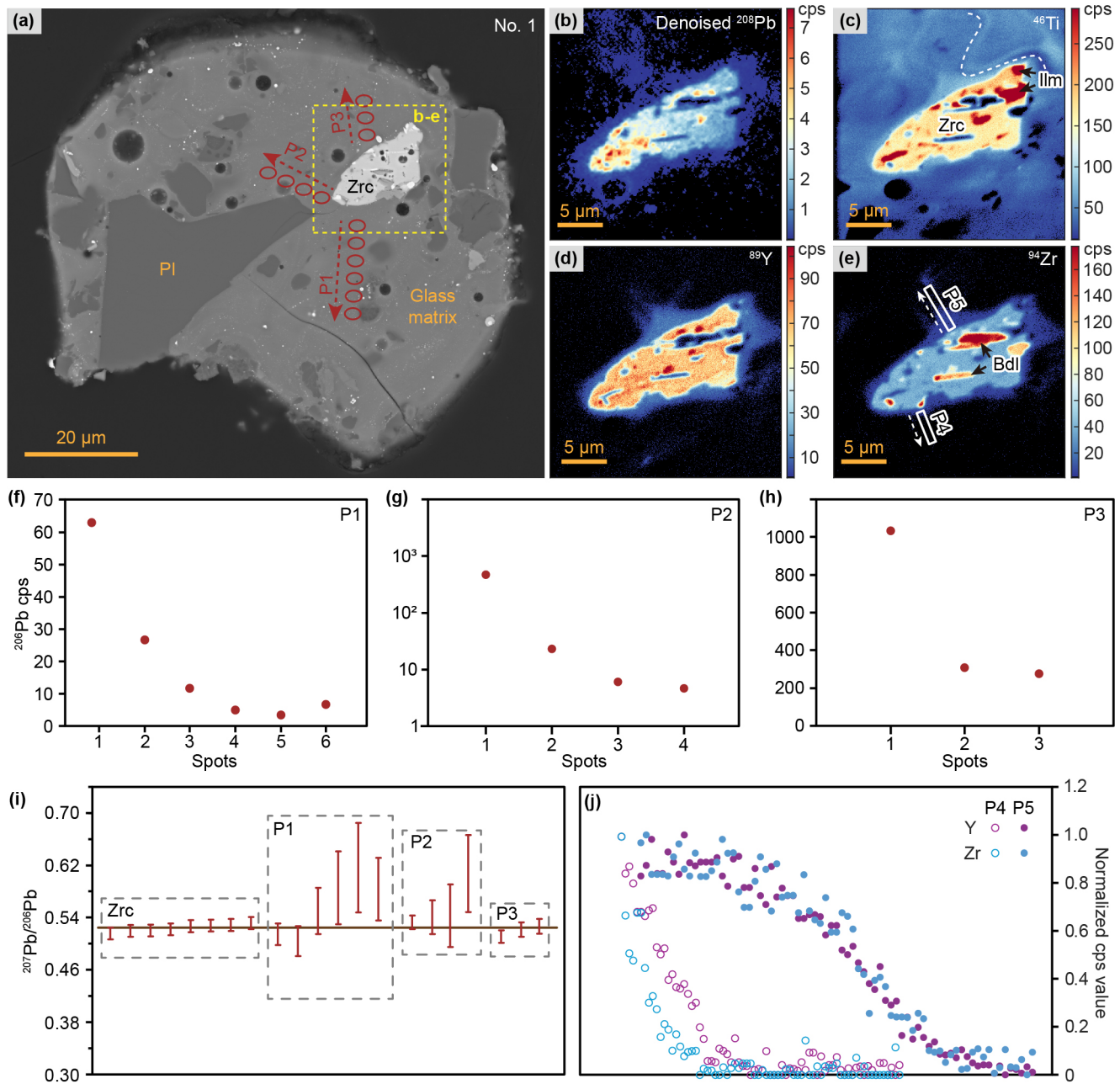


Fig. 8 Pb isotope data of the glass matrix and Nano-SIMS mapping results. **a** BSE image of bead No. 1 showing three profiles of SIMS spot analyses (P1–P3) (red dotted lines and ellipses) and the Nano-SIMS mapping region (yellow dashed rectangle). **b–e** Nano-SIMS maps of relative content of ^{208}Pb , ^{46}Ti , ^{89}Y , and ^{94}Zr , respectively. The positions of two profiles, P4 (3.5 μm) and P5 (5 μm), extracted from the Nano-SIMS maps are shown in **e**. The colour scale limits were adjusted to

emphasize chemical variations at low cps; as a result, regions with higher cps values exceeding the upper limit are displayed using the final colour of the bar. **f–h** ^{208}Pb counts per second (cps) values for spots along the three profiles (P1–P3). **i** Comparison of $^{207}\text{Pb}/^{206}\text{Pb}$ ratios between the zirconite crystal and the glass matrix. **j** Extracted cps values of ^{89}Y and ^{94}Zr along the profiles (P4–P5) in Nano-SIMS maps indicated in **e**, normalized from 0 to 1

lunar soils are predominantly composed of locally derived basaltic materials. This is further supported by geochemical analyses of the returned bulk soils and homogeneous impact glass beads (Long et al. 2022; Yang et al. 2022; Zong et al. 2022). Only a few exotic clasts and glasses, ejected from the lunar highlands or other mare regions, have been

identified based on their petrographic features and mineral compositions (Long et al. 2022; Zeng et al. 2023). As direct products of impact gardening, glass beads containing abundant undigested minerals offer valuable insights into exotic lunar materials beyond the sampling site. Furthermore, undigested zirconium-containing minerals can be used to

determine their formation ages, providing additional chronological constraints on their provenances.

The pristine crystallization age of zirconolite in glass bead No. 1 (Fig. 2b) is 4310 ± 13 Ma, which is significantly older than the ages of most mare basalts in lunar records (e.g., Borg et al. 2009; Merle et al. 2024; Shearer et al. 2023; Snape et al. 2016; Zhang et al. 2024). Combined with the composition of most undigested plagioclase, with X_{An} values between 0.83 and 0.88 (Fig. 6a), and olivine with $Mg\#$ [=molar $Mg/(Mg+Fe)$] values between 0.51 and 0.61 (Supplementary Table S4), this glass bead is likely derived from the melting of highland materials dominated by alkali-suite rocks (Prissel and Gross 2020). The presence of a few high-Ca plagioclase crystals with $X_{An} > 0.95$ (Fig. 6a) suggests the involvement of other highland materials (Fig. 9a), such as anorthosite or Mg-suite rocks (Prissel and Gross 2020). Therefore, bead No. 1 likely represents an exotic grain ejected from the lunar highlands and deposited at the Chang'e 5 sampling site.

The concordant age of the undigested zircon core in glass bead No. 2 (Fig. 2d) is 3921 ± 14 Ma, significantly older than the age of the Chang'e-5 basalt (2.0 Ga) (Che et al. 2021; Li et al. 2021), indicating an exotic origin for this bead. Similar ages have been reported from the Apollo high-Al basalts (Snape et al. 2016, 2019) and lunar basaltic meteorites (Merle et al. 2024), representing the oldest mare volcanism on the Moon. One undigested plagioclase crystal in this bead shows compositional zoning with the X_{An} values ranging from 0.83 to 0.89 (Fig. 6b), consistent with a basalt origin. Therefore, we interpret this bead as having been ejected from an ancient basaltic region with an age of ~ 3.9 Ga.

The age of the undigested zircon crystal in glass bead No. 3 (Fig. 2f) is 2043 ± 53 Ma, which is consistent with the previously reported formation age of Chang'e-5 basalt as determined by Pb-Pb isochron dating of basalt fragments (Boschi et al. 2023; Che et al. 2021; Hao et al. 2024; Li et al. 2021) and zircon crystals (Zhou et al. 2023), within uncertainties. Most undigested plagioclase crystals show X_{An} values between 0.76 and 0.86, comparable to those in Chang'e-5 basalt (Li et al. 2023). The presence of undigested quartz (Fig. 2e) in this bead is consistent with the highly evolved petrographic features of Chang'e-5 basalt, reflecting a high degree of fractionation crystallization. Therefore, we suggest that the melting materials of this bead are predominantly derived from local mare basalt materials from the Chang'e-5 landing region.

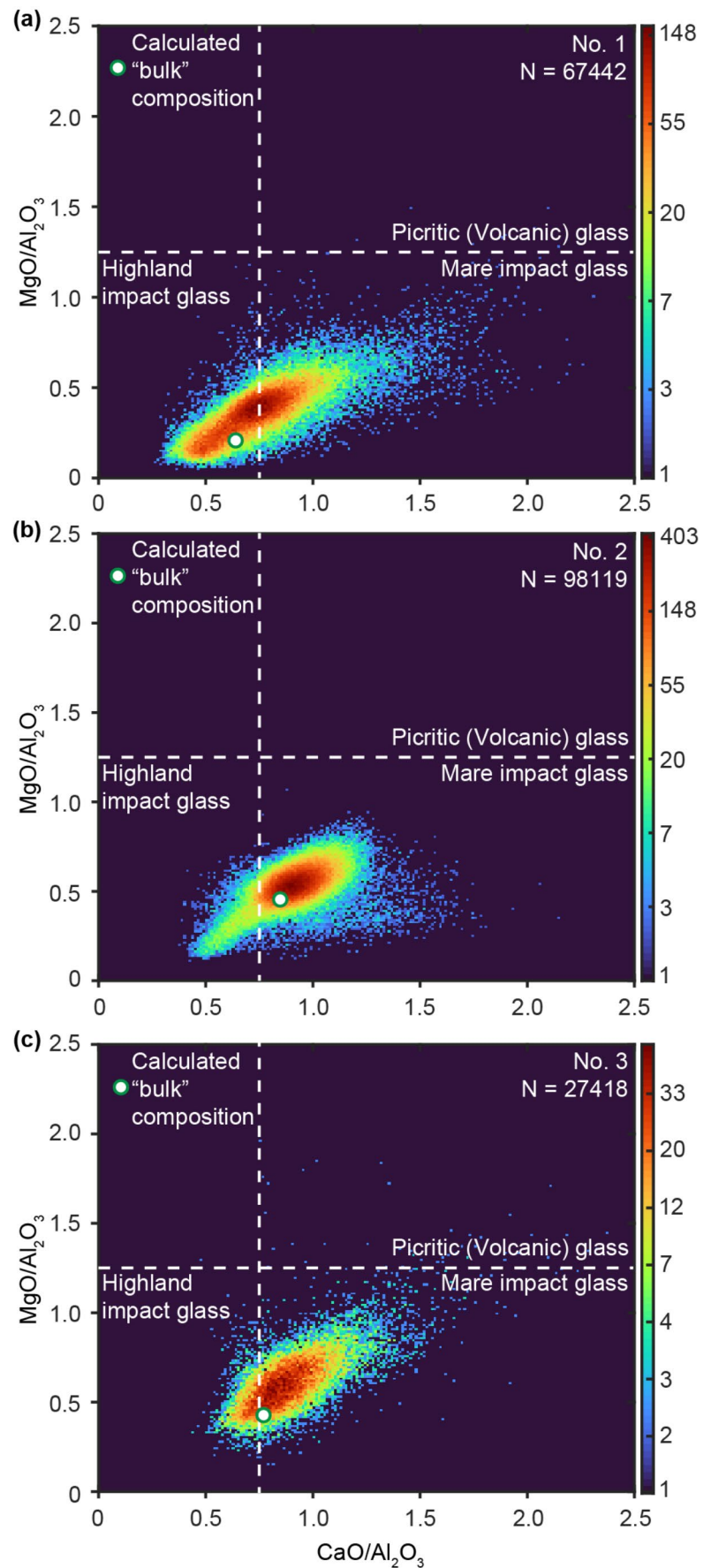
Complexity and pitfalls of major element compositions of glass matrix

The MgO/Al_2O_3 and CaO/Al_2O_3 ratios are widely used to distinguish different origins of glasses, with an MgO/Al_2O_3 ratio of 1.25 serving as boundary between volcanic and impact glass beads, and a CaO/Al_2O_3 ratio of 0.75 as the boundary between highland-origin and mare-origin impact glass beads (Delano 1986; Delano et al. 2007; Naney et al. 1976; Zeigler et al. 2006). As shown in the EPMA and NanoSIMS mapping results, the compositions of major elements (such as Ca, Al, Mg, Fe, etc.) and trace elements (such as Ti, Y, Zr, Pb, etc.) in the glass matrix exhibit significant variations (Figs. 3, 4, 5, 8), indicating incomplete melting and homogenization. These compositional complexities present a challenge in obtaining a representative composition of the entire glass bead using traditional in-situ microanalytical methods.

The major element composition data extracted from the pixels in the EPMA mapping of the glass matrices in all three heterogeneous glass beads consistently show low MgO/Al_2O_3 ratios (< 1.25), placing them in the region of impact glass. However, their CaO/Al_2O_3 ratios vary widely (mostly between 0.3 and 1.5), spanning both highland-impact and mare-impact regions on the widely used discrimination diagram (Fig. 9). Variations in Al_2O_3 contents and CaO/Al_2O_3 ratios in partial glass matrix are spatially correlated with the distance from undigested plagioclase crystals within the matrix (Figs. 3, 4, 5). Consequently, the major element compositions obtained from EPMA spot analyses of local regions within the heterogeneous glass matrix of a single bead show inconsistent provenance interpretations (Fig. 9), which contradicts the geochronological and compositional features of the undigested minerals.

By integrating the composition of each pixel and accounting for the density of each mineral species, the bulk composition of the entire glass bead can be calculated from quantitative maps (Lanari and Engi 2017) (Supplementary Table S5). Glass bead No. 1, containing ~ 4.31 Ga zirconolite, exhibits a bulk composition with a CaO/Al_2O_3 ratio of 0.64 and MgO/Al_2O_3 ratio of 0.21, indicative of a highland impact origin. The other two glass beads, No. 2 and No. 3, containing ~ 3.92 Ga and ~ 2.04 Ga zircon, respectively, show bulk compositions characteristic of mare impact origins, with CaO/Al_2O_3 ratios of 0.85 and 0.77 (Fig. 9). The provenances indicated by these bulk compositions are consistent with those inferred from the ages of the zirconium-bearing minerals and the compositions of undigested minerals.

Fig. 9 Density plot of $\text{MgO}/\text{Al}_2\text{O}_3$ and $\text{CaO}/\text{Al}_2\text{O}_3$ ratios of pixels extracted from the mapping results of the glass matrices in the three glass beads Nos. 1–3. The horizontal dashed line indicates $\text{MgO}/\text{Al}_2\text{O}_3 = 1.25$, separating volcanic glass beads (above) and impact glasses (below), and the vertical dashed line denotes $\text{CaO}/\text{Al}_2\text{O}_3 = 0.75$, distinguishing highland impact glasses (left) from mare impact glasses (right) (Delano 1986; Delano et al. 2007; Naney et al. 1976; Zeigler et al. 2006)



Diffusion-controlled elemental distribution

SIMS Pb isotope analyses of the glass matrix reveal that ^{206}Pb abundances, indicated by counts per second (cps) values of ^{206}Pb , decrease gradually outward from the zirconolite crystal along all three profiles (Fig. 8f–h). We propose that this decreasing trend results from the diffusion of Pb released by the partially melted zirconolite under the high-temperature conditions associated with the impact. Multiple lines of evidence support the partial melting of the precursor zirconolite: (1) the preserved zirconolite, in direct contact with the glass matrix, shows smooth edges and lacks the straight boundaries typical of pristine crystals (Fig. 2b). (2) The presence of baddeleyite as tiny grains along the edges of zirconolite or as exsolution bands within zirconolite indicates a high-temperature conversion process during impact melting (Loiseau et al. 2003; Zhang et al. 2011). Notably, the $^{207}\text{Pb}/^{206}\text{Pb}$ ratios of most spots on the glass matrix are consistent with those of zirconolite (Fig. 8i), indicating that the glass matrix inherits the Pb isotope composition of the partially melted zirconolite and that there is no isotope fractionation during the high-temperature diffusion process. Some spots farther from the zirconolite exhibit higher $^{207}\text{Pb}/^{206}\text{Pb}$ ratios (Fig. 8i), likely due to the involvement of Pb from other silicate minerals, such as plagioclase and pyroxene, which contain higher $^{207}\text{Pb}/^{206}\text{Pb}$ ratios of non-radiogenic initial Pb (Li et al. 2021).

Nano-SIMS maps reveal clear enrichments of ^{46}Ti , ^{89}Y , and ^{94}Zr in the glass matrix surrounding the undigested zirconolite (Fig. 8c–e). Most profiles extracted from the glass matrix surrounding the undigested zirconolite exhibit compositional gradients consistent with diffusion-controlled transport. For example, profile P4 (Fig. 8e) exhibits a smooth, monotonic decrease in the concentrations of ^{89}Y and ^{94}Zr with increasing distance from the zirconolite (Fig. 8j). The difference in the curvature of ^{89}Y and ^{94}Zr profiles corresponds to the expected difference in diffusion coefficients between Y and Zr (Holycross and Watson 2016), indicating a typical diffusion profile (Liu et al. 2025). These lines of evidence confirm diffusion-controlled compositional complexity in the heterogeneous glass beads during the incomplete melting of involved regolith materials. Along another profile P5, the Y and Zr abundances generally show a decreasing trend, however, both elements exhibit significant fluctuations, and no clear difference in curvature is observed between their profiles. These features, combined with the streamlined chemical patterns observed in the Nano-SIMS and EPMA maps (e.g., Figs. 4f, 8c–e), suggest the additional influence of localized melt convection within the droplet. We interpret these mixed profiles as the result of a combined effect of diffusion and convective transport during the rapid

solidification of impact melt, which further complicates the heterogeneity of the glass matrix.

Implications for U–Pb dating of glass beads

Impact glass beads serve as direct time capsules of lunar impact events. $^{40}\text{Ar}/^{39}\text{Ar}$ and U–Pb dating of these glasses can be used to determine the timing of individual impact events, offering critical insights into the bombardment history of the Moon and, by extension, the Earth–Moon system (Culler et al. 2000; Delano et al. 2007; Levine et al. 2005; Long et al. 2022; Nemchin et al. 2022; Norman et al. 2012, 2019). In this context, the target of geochronology is the formation age of the glass itself, rather than that of relict minerals it may contain. To accurately date the glass beads using SIMS U–Pb method, it is essential to correct for the proportion and isotopic composition of common Pb, which is not accumulated from in-situ U–Th decay post-formation but inherited from precursor regolith materials (Long et al. 2022; Nemchin et al. 2022; Norman et al. 2012).

Homogeneous glass beads likely experienced significant Pb volatilization during impact melting and quenching, leading to substantial Pb loss and a homogenized common Pb isotopic composition that reflects an average of the regolith-derived melt. In contrast, heterogeneous beads retain Pb compositions that were not fully volatilized or homogenized, with its distribution largely controlled by the presence of undigested mineral phases exhibiting variable Pb abundances. Residual minerals with inherently higher Pb abundances—such as zirconolite, baddeleyite, and zircon—exert a greater influence on the Pb isotopic composition of the surrounding glass matrix than Pb-poor silicate phases. The present SIMS Pb isotope analyses and Nano-SIMS maps on the glass matrix surrounding the ~ 4.31 Ga zirconolite confirm that the high proportions of common Pb in these glasses originate from the partially melted zirconolite crystal through Pb diffusion. Although this Pb distribution mechanism is demonstrated in heterogeneous glass beads containing Zr-bearing minerals, we propose that the Pb isotopic compositions of other heterogeneous beads—with abundant relict silicate phases—are also largely influenced by the residual minerals due to higher $^{207}\text{Pb}/^{206}\text{Pb}$ ratios in the common Pb component.

Correcting for common Pb in heterogeneous glass beads is challenging due to the unpredictable Pb isotope composition of precursor minerals and the amount of Pb lost from the molten droplet. A recent geochronological study, combined with multi-disciplinary modelling of impact melt generation and migration of various Chang'e-5 impact glass beads, has revealed that heterogeneous beads often exhibit elevated $^{207}\text{Pb}/^{206}\text{Pb}$ ratios and lower $^{238}\text{U}/^{206}\text{Pb}$ ratios compared to their homogeneous counterparts, suggesting

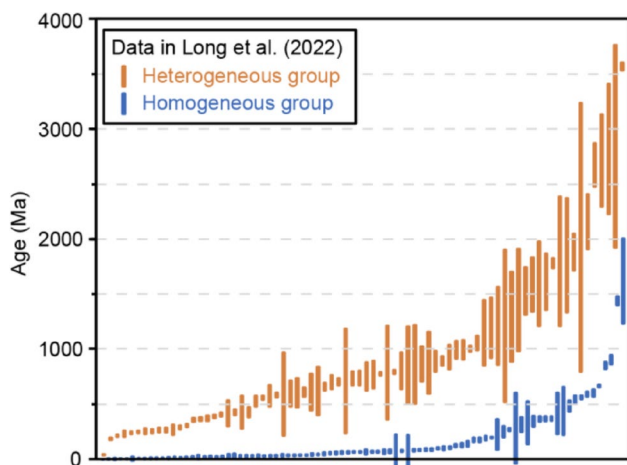


Fig. 10 Comparison of common-Pb corrected age results between heterogeneous (yellow) and homogeneous glass beads (blue) reported by Long et al. (2022)

elevated levels of common Pb (Fig. 3A, B in Long et al. 2022). Moreover, the age distributions of heterogeneous beads (Long et al. 2022) show a higher proportion of older ages compared to homogeneous beads (Fig. 10), which may suggest a potential bias, possibly related to the inadequate correction of common Pb inherited from precursor minerals. This bias significantly undermines the accuracy of the age frequency distribution derived from the integrated age dataset of impact glass beads. Consequently, we recommend homogeneous glass beads with low proportions of common Pb as best targets in the future U–Pb dating studies.

Conclusions

Heterogeneous glass beads are the predominant glass type in lunar soils and have been widely used for in-situ microanalysis in geochemical studies. We analysed three heterogeneous glass beads containing undigested zirconolite and zircon using EPMA and Nano-SIMS mapping, as well as SIMS U–Pb isotope analyses, to illustrate the compositional complexity of these beads. The undigested zirconolite and zircon crystals within the beads record three distinct volcanic events that contributed to the evolution of lunar crust: ~4.31 Ga alkali-suite rocks in the highlands, ~3.92 Ga, and ~2.04 Ga mare basalts. This indicates that the U–Pb system in the undigested zircon and zirconolite crystals in impact glass beads remains undisturbed during the ultra-high-temperature, short-duration melting events. EPMA mapping highlights the compositional inhomogeneity of the glass matrices, which prevents an accurate representation of their origins through in-situ microanalysis. The bulk composition reconstructed based on quantitative maps, however, offers a more reliable reference for determining provenance. The

high proportions of common Pb in the heterogeneous glass matrix, originating from partially melted minerals through diffusion-controlled processes, lead to significant uncertainties in U–Pb dating of impact events.

Supplementary Information The online version contains supplementary material available at <https://doi.org/10.1007/s00410-025-02220-w>.

Acknowledgements This study was financially supported by the National Natural Science Foundation of China (42225301, 42241105, 42403008), the Key Research Program of the Institute of Geology and Geophysics, Chinese Academy of Sciences (IGGCAS-202401), and China National Postdoctoral Program for Innovative Talents (BX20220294).

Data availability The relevant data are given in supplementary data.

Declarations

Conflict of interest The authors declare that they have no potential conflict of interest that could have appeared to influence the work reported in this paper.

Open Access This article is licensed under a Creative Commons Attribution 4.0 International License, which permits use, sharing, adaptation, distribution and reproduction in any medium or format, as long as you give appropriate credit to the original author(s) and the source, provide a link to the Creative Commons licence, and indicate if changes were made. The images or other third party material in this article are included in the article's Creative Commons licence, unless indicated otherwise in a credit line to the material. If material is not included in the article's Creative Commons licence and your intended use is not permitted by statutory regulation or exceeds the permitted use, you will need to obtain permission directly from the copyright holder. To view a copy of this licence, visit <http://creativecommons.org/licenses/by/4.0/>.

References

- Adams JB, Charette MP, Rhodes JM (1975) Chemical fractionation of the lunar regolith by impact melting. *Science* 190:380–381. <https://doi.org/10.1126/science.190.4212.380>
- Arndt J, Engelhardt WV, Gonzalez-Cabeza I, Meier B (1984) Formation of Apollo 15 green glass beads. *J Geophys Res Solid Earth* 89:C225–C232. <https://doi.org/10.1029/JB089iS01p0C225>
- Baker J, Peate D, Waight T, Meyzen C (2004) Pb isotopic analysis of standards and samples using a ^{207}Pb – ^{204}Pb double Spike and thallium to correct for mass bias with a double-focusing MC–ICP–MS. *Chem Geol* 211:275–303. <https://doi.org/10.1016/j.chemgeo.2004.06.030>
- Barboni M, Szymanowski D, Schoene B, Dauphas N, Zhang ZJ, Chen X, McKeegan KD (2024) High-precision U–Pb zircon dating identifies a major magmatic event on the Moon at 4.338 Ga. *Sci Adv* 10:eadn9871. <https://doi.org/10.1126/sciadv.adn9871>
- Bischoff A, Stöffler D (1992) Shock metamorphism as a fundamental process in the evolution of planetary bodies: information from meteorites. *Eur J Mineral* 4:707–755. <https://doi.org/10.1127/ejm/4/4/0707>
- Borg LE, Gaffney AM, Shearer CK, DePaolo DJ, Hutcheon ID, Owens TL, Ramon E, Brennecka G (2009) Mechanisms for

- incompatible-element enrichment on the Moon deduced from the lunar basaltic meteorite Northwest Africa 032. *Geochim Cosmochim Acta* 73:3963–3980. <https://doi.org/10.1016/j.gca.2009.03.039>
- Boschi S, Wang XL, Hui H, Yin Z, Guan Y, Hu H, Zhang W, Chen J, Li W (2023) Compositional variability of 2.0-Ga lunar basalts at the Chang'e-5 landing site. *J Geophys Res Planets* 128:e2022JE007627. <https://doi.org/10.1029/2022je007627>
- Chao ECT, Boreman JA, Minkin JA, James OB, Desborough GA (1970) Lunar glasses of impact origin: physical and chemical characteristics and geologic implications. *J Geophys Res* 75:7445–7479. <https://doi.org/10.1029/JB075i035p07445>
- Che X, Nemchin A, Liu D, Long T, Wang C, Norman MD, Joy KH, Tartese R, Head J, Jolliff B, Snape JF, Neal CR, Whitehouse MJ, Crow C, Benedix G, Jourdan F, Yang Z, Yang C, Liu J, Xie S, Bao Z, Fan R, Li D, Li Z, Webb SG (2021) Age and composition of young basalts on the Moon, measured from samples returned by Chang'e-5. *Science* 374:887–890. <https://doi.org/10.1126/science.abl7957>
- Chen Y, Hu S, Li JH, Li QL, Li XY, Li Y, Liu Y, Qian YQ, Yang W, Zhou Q, Lin YT, Li CL, Li XH (2023) Chang'e-5 lunar samples shed new light on the Moon. *Innov Geosci* 1:100014. <https://doi.org/10.59717/j.xinn-geo.2023.100014>
- Cherniak DJ, Watson EB (2001) Pb diffusion in Zircon. *Chem Geol* 172:5–24. [https://doi.org/10.1016/S0009-2541\(00\)00233-3](https://doi.org/10.1016/S0009-2541(00)00233-3)
- Cintala MJ, Grieve RAF (1998) Scaling impact melting and crater dimensions: implications for the lunar cratering record. *Meteorit Planet Sci* 33:889–912. <https://doi.org/10.1111/j.1945-5100.1998.tb01695.x>
- Culler TS, Becker TA, Muller RA, Renne PR (2000) Lunar impact history from $^{40}\text{Ar}/^{39}\text{Ar}$ dating of glass spherules. *Science* 287:1785–1788. <https://doi.org/10.1126/science.287.5459.1785>
- Delano JW (1986) Pristine lunar glasses: criteria, data, and implications. *J Geophys Res Solid Earth* 91:201–213. <https://doi.org/10.1029/JB091iB04p0D201>
- Delano JW (1991) Geochemical comparison of impact glasses from lunar meteorites ALHA81005 and MAC88105 and Apollo 16 regolith 64001. *Geochim Cosmochim Acta* 55:3019–3029. [https://doi.org/10.1016/0016-7037\(91\)90470-P](https://doi.org/10.1016/0016-7037(91)90470-P)
- Delano JW, Lindsley DH, Rudowski R (1981) Glasses of impact origin from Apollo 11, 12, 15, and 16: evidence for fractional vaporization and mare/highland mixing. *Lunar Planet Sci Conf Proc* 12:339–370
- Delano JW, Zellner NEB, Barra F, Olson E, Swindle TD, Tibbetts NJ, Whittet DCB (2007) An integrated approach to Understanding Apollo 16 impact glasses: chemistry, isotopes, and shape. *Meteorit Planet Sci* 42:993–1004. <https://doi.org/10.1111/j.1945-5100.2007.tb01146.x>
- Ganguly J, Tirone M (1999) Diffusion closure temperature and age of a mineral with arbitrary extent of diffusion: theoretical formulation and applications. *Earth Planet Sci Lett* 170:131–140. [https://doi.org/10.1016/S0012-821X\(99\)00089-8](https://doi.org/10.1016/S0012-821X(99)00089-8)
- Grange ML, Nemchin AA, Pidgeon RT, Timms N, Muhling JR, Kennedy AK (2009) Thermal history recorded by the Apollo 17 impact melt breccia 73217. *Geochim Cosmochim Acta* 73:3093–3107. <https://doi.org/10.1016/j.gca.2009.02.032>
- Hao J-L, Yang W, Luo Y, Hu S, Yin Q-Z, Lin Y-T (2016) NanoSIMS measurements of trace elements at the micron scale interface between Zircon and silicate glass. *J Anal Spectrom* 31:2399–2409. <https://doi.org/10.1039/c6ja00279j>
- Hao J-L, Yang W, Hu S, Li R-Y, Ji J-L, Changela HG, Lin Y-T (2021) Submicron Spatial resolution Pb–Pb and U–Pb dating by using a nanosims equipped with the new radio-frequency ion source. *J Anal Spectrom* 36:1625–1633. <https://doi.org/10.1039/d1ja00085c>
- Hao J-L, Yang W, He H-C, Zhang D, Hu S, Tian H-C, Li R-Y, Lin Y-T (2024) Submicron Spatial resolution Pb–Pb dating for the formation age of Chang'e-5 basalt. *Lithos* 468–469:107495. <https://doi.org/10.1016/j.lithos.2024.107495>
- He H, Ji J, Zhang Y, Hu S, Lin Y, Hui H, Hao J, Li R, Yang W, Tian H, Zhang C, Anand M, Tartese R, Gu L, Li J, Zhang D, Mao Q, Jia L, Li X, Chen Y, Zhang L, Ni H, Wu S, Wang H, Li Q, He H, Li X, Wu F (2023) A solar wind-derived water reservoir on the Moon hosted by impact glass beads. *Nat Geosci* 16:294–300. <https://doi.org/10.1038/s41561-023-01159-6>
- Heaman LM (2009) The application of U–Pb geochronology to mafic, ultramafic and alkaline rocks: an evaluation of three mineral standards. *Chem Geol* 261:43–52. <https://doi.org/10.1016/j.chemgeo.2008.10.021>
- Holycross ME, Watson BE (2016) Diffusive fractionation of trace elements in basaltic melt. *Contrib Mineral Petrol* 171:80. <https://doi.org/10.1007/s00410-016-1289-x>
- Korotev RL, Zeigler RA, Floss C (2010) On the origin of impact glass in the Apollo 16 regolith. *Geochim Cosmochim Acta* 74:7362–7388. <https://doi.org/10.1016/j.gca.2010.09.020>
- Lanari P, Engi M (2017) Local bulk composition effects on metamorphic mineral assemblages. *Rev Mineral Geochem* 83:55–102. <https://doi.org/10.2138/rmg.2017.83.3>
- Lanari P, Tedeschi M (2025) Chemical map classification in xmaptools. *Appl Comput Geosci* 25:100230. <https://doi.org/10.1016/j.acags.2025.100230>
- Lanari P, Vidal O, De Andrade V, Dubacq B, Lewin E, Grosch EG, Schwartz S (2014) XMapTools: a MATLAB[®]-based program for electron microprobe X-ray image processing and geothermobarometry. *Comput Geosci* 62:227–240. <https://doi.org/10.1016/j.cageo.2013.08.010>
- Lanari P, Vho A, Bovay T, Airaghi L, Centrella S (2019) Quantitative compositional mapping of mineral phases by electron probe micro-analyser. *Geol Soc Lond Spec Publ* 478:39–63. <https://doi.org/10.1144/sp478.4>
- Levine J, Becker TA, Muller RA, Renne PR (2005) $^{40}\text{Ar}/^{39}\text{Ar}$ dating of Apollo 12 impact spherules. *Geophys Res Lett* 32:L15201. <https://doi.org/10.1029/2005GL022874>
- Li Q-L, Li X-H, Liu Y, Tang G-Q, Yang J-H, Zhu W-G (2010) Precise U–Pb and Pb–Pb dating of phanerozoic baddeleyite by SIMS with oxygen flooding technique. *J Anal Spectrom* 25:1107–1113. <https://doi.org/10.1039/b923444f>
- Li XH, Tang GQ, Gong B, Yang YH, Hou KJ, Hu ZC, Li QL, Liu Y, Li WX (2013) Qinghu Zircon: a working reference for microbeam analysis of U–Pb age and Hf and O isotopes. *Chin Sci Bull* 58:4647–4654. <https://doi.org/10.1007/s11434-013-5932-x>
- Li QL, Zhou Q, Liu Y, Xiao Z, Lin Y, Li JH, Ma HX, Tang GQ, Guo S, Tang X, Yuan JY, Li J, Wu FY, Ouyang Z, Li C, Li XH (2021) Two-billion-year-old volcanism on the Moon from Chang'e-5 basalts. *Nature* 600:54–58. <https://doi.org/10.1038/s41586-021-04100-2>
- Li CL, Hu H, Yang MF, Pei ZY, Zhou Q, Ren X, Liu B, Liu DW, Zeng XG, Zhang GL, Zhang HB, Liu JJ, Wang Q, Deng XJ, Xiao CJ, Yao YG, Xue DS, Zuo W, Su Y, Wen WB, Ouyang ZY (2022) Characteristics of the lunar samples returned by the Chang'e-5 mission. *Natl Sci Rev* 9:nwab188. <https://doi.org/10.1093/nsr/nwab188>
- Li L, Hui H, Hu S, Wang H, Yang W, Chen Y, Wu S, Gu L, Jia L, Wu F (2023) Petrogenesis of Chang'e-5 young mare low-Ti basalts. *Meteorit Planet Sci* 58:1429–1448. <https://doi.org/10.1111/maps.14071>
- Liu Y, Guan Y, Zhang Y, Rossman GR, Eiler JM, Taylor LA (2012) Direct measurement of hydroxyl in the lunar regolith and the origin of lunar surface water. *Nat Geosci* 5:779–782. <https://doi.org/10.1038/ngeo1601>

- Liu Y, Li X-H, Li Q-L, Tang G-Q (2020) Breakthrough of 2- to 3- μm scale U–Pb Zircon dating using Cameca IMS-1280HR SIMS. *Surf Interface Anal* 52:214–223. <https://doi.org/10.1002/sia.6752>
- Liu J-H, Lanari P, Tamblyn R, Dominguez H, Hermann J, Rubatto D, Forshaw JB, Piccoli F, Zhang QWL, Markmann TA, Reynes J, Li ZMG, Jiao S, Guo J (2025) Ultra-fast metamorphic reaction during regional metamorphism. *Geochim Cosmochim Acta* 394:106–125. <https://doi.org/10.1016/j.gca.2025.01.036>
- Loiseau P, Caurant D, Majerus O, Baffier N, Fillet C (2003) Crystallization study of (TiO₂, ZrO₂)-rich SiO₂–Al₂O₃–CaO glasses part II surface and internal crystallization processes investigated by differential thermal analysis (DTA). *J Mater Sci* 38:853–864. <http://doi.org/10.1023/A:1021825418336>
- Long T, Qian YQ, Norman MD, Miljkovic K, Crow C, Head JW, Che XC, Tartèse R, Zellner N, Yu XF, Xie SW, Whitehouse M, Joy KH, Neal CR, Snape JF, Zhou GS, Liu SJ, Yang C, Yang ZQ, Wang C, Xiao L, Liu DY, Nemchin A (2022) Constraining the formation and transport of lunar impact glasses using the ages and chemical compositions of Chang'e-5 glass beads. *Sci Adv* 8:eabq2542. <https://doi.org/10.1126/sciadv.abq2542>
- Ludwig KR (2008) Isoplot 3.6: a geochronological toolkit for Microsoft Excel. Berkeley Geochronol Cent Special Publication 4:1
- Manske L, Wünnemann K, Kurosawa K (2022) Quantification of impact-induced melt production in numerical modeling revisited. *J Geophys Res Planet* 127:e2022JE007426. <https://doi.org/10.1029/2022je007426>
- Merle RE, Nemchin AA, Whitehouse MJ, Kenny GG, Snape JF (2024) Pb isotope signature of a low- μ (²³⁸U/²⁰⁴Pb) lunar mantle component. *J Petrol* 65:egae062. <https://doi.org/10.1093/petrology/egae062>
- Morris RV (1978) In situ reworking (gardening) of the lunar surface: evidence from the Apollo cores. *Lunar Planet Sci Conf* 9:1801–1811
- Naney MT, Crowl DM, Papike JJ (1976) The Apollo 16 drill core: statistical analysis of glass chemistry and the characterization of a high alumina-silica poor (HASP) glass. *Lunar Planet Sci Conf Proc* 7:155–184
- Nemchin AA, Pidgeon RT, Whitehouse MJ, Vaughan JP, Meyer C (2008) SIMS U–Pb study of Zircon from Apollo 14 and 17 breccias: implications for the evolution of lunar KREEP. *Geochim Cosmochim Acta* 72:668–689. <https://doi.org/10.1016/j.gca.2007.11.009>
- Nemchin A, Timms N, Pidgeon R, Geisler T, Reddy S, Meyer C (2009) Timing of crystallization of the lunar magma ocean constrained by the oldest Zircon. *Nat Geosci* 2:133–136. <https://doi.org/10.1038/ngeo417>
- Nemchin AA, Grange ML, Pidgeon RT, Meyer C (2012) Lunar zirconology. *Aust J Earth Sci* 59:277–290. <https://doi.org/10.1080/08120099.2011.613484>
- Nemchin AA, Norman MD, Grange ML, Zeigler RA, Whitehouse MJ, Muhling JR, Merle R (2022) U–Pb isotope systematics and impact ages recorded by a chemically diverse population of glasses from an Apollo 14 lunar soil. *Geochim Cosmochim Acta* 321:206–243. <https://doi.org/10.1016/j.gca.2021.12.013>
- Norman MD, Nemchin AA (2014) A 4.2 billion year old impact basin on the Moon: U–Pb dating of zirconolite and apatite in lunar melt rock 67955. *Earth Planet Sci Lett* 388:387–398. <https://doi.org/10.1016/j.epsl.2013.11.040>
- Norman MD, Adena KJD, Christy AG (2012) Provenance and Pb isotopic ages of lunar volcanic and impact glasses from the Apollo 17 landing site. *Aust J Earth Sci* 59:291–306. <https://doi.org/10.1080/08120099.2011.615471>
- Norman MD, Jourdan F, Hui SSM (2019) Impact history and regolith evolution on the Moon: geochemistry and ages of glasses from the Apollo 16 site. *J Geophys Res Planet* 124:3167–3180. <https://doi.org/10.1029/2019je006053>
- Prissel TC, Gross J (2020) On the petrogenesis of lunar troctolites: new insights into cumulate mantle overturn and mantle exposures in impact basins. *Earth Planet Sci Lett* 551:116531. <https://doi.org/10.1016/j.epsl.2020.116531>
- Ryder G, Spudis P (1987) Chemical composition and origin of Apollo 15 impact melts. *J Geophys Res Solid Earth* 92:E432–E446. <http://doi.org/10.1029/JB092iB04p0E432>
- Shearer C, Neal CR, Glotch TD, Prissel TC, Bell AS, Fernandes VA, Gaddis LR, Jolliff BL, Laneuville M, Magna T, Simon J (2023) Magmatic evolution II: a new view of post-differentiation magmatism. *Rev Mineral Geochem* 89:147–206. <https://doi.org/10.2138/rmg.2023.89.04>
- Simon SB, Papike JJ, Laul JC (1981) The lunar regolith: comparative studies of the Apollo and Luna sites. *Petrology of soils from Apollo 17, Luna 16, 20, and 24. Lunar and Planetary Science Conference Proceedings* 12:371–388
- Sláma J, Košler J, Condon DJ, Crowley JL, Gerdes A, Hanchar JM, Horstwood MSA, Morris GA, Nasdala L, Norberg N, Schaltegger U, Schoene B, Tubrett MN, Whitehouse MJ (2008) Plešovice Zircon: a new natural reference material for U–Pb and Hf isotopic microanalysis. *Chem Geol* 249:1–35. <https://doi.org/10.1016/j.chemgeo.2007.11.005>
- Snape JF, Nemchin AA, Bellucci JJ, Whitehouse MJ, Tartèse R, Barnes JJ, Anand M, Crawford IA, Joy KH (2016) Lunar basalt chronology, mantle differentiation and implications for determining the age of the Moon. *Earth Planet Sci Lett* 451:149–158. <https://doi.org/10.1016/j.epsl.2016.07.026>
- Snape JF, Nemchin AA, Whitehouse MJ, Merle RE, Hopkinson T, Anand M (2019) The timing of basaltic volcanism at the Apollo landing sites. *Geochim Cosmochim Acta* 266:29–53. <https://doi.org/10.1016/j.gca.2019.07.042>
- Wang B-W, Zhang QWL, Chen Y, Zhao W, Liu Y, Tang G-Q, Ma H-X, Su B, Hui H, Delano JW, Wu F-Y, Li X-H, He Y, Li Q-L (2024) Returned samples indicate volcanism on the Moon 120 million years ago. *Science* 385:1077–1080. <https://doi.org/10.1126/science.adk6635>
- Warr LN (2021) IMA–CNMNC approved mineral symbols. *Mineral Mag* 85:291–320. <https://doi.org/10.1180/mgm.2021.43>
- Wu F-Y, Yang Y-H, Mitchell RH, Bellatreccia F, Li Q-L, Zhao Z-F (2010) In situ U–Pb and Nd–Hf–(Sr) isotopic investigations of zirconolite and calzirtite. *Chem Geol* 277:178–195. <https://doi.org/10.1016/j.chemgeo.2010.08.007>
- Yang W, Chen Y, Wang H, Tian HC, Hui HJ, Xiao ZY, Wu ST, Zhang D, Zhou Q, Ma HX, Zhang C, Hu S, Li QL, Lin YT, Li XH, Wu FY (2022) Geochemistry of impact glasses in the Chang'e-5 regolith: constraints on impact melting and the petrogenesis of local basalt. *Geochim Cosmochim Acta* 335:183–196. <https://doi.org/10.1016/j.gca.2022.08.030>
- Zeigler RA, Korotev RL, Jolliff BL, Haskin LA, Floss C (2006) The geochemistry and provenance of Apollo 16 mafic glasses. *Geochim Cosmochim Acta* 70:6050–6067. <https://doi.org/10.1016/j.gca.2006.08.040>
- Zellner NEB (2019) Lunar impact glasses: probing the Moon's surface and constraining its impact history. *J Geophys Res Planet* 124:2686–2702. <https://doi.org/10.1029/2019JE006050>
- Zeng XJ, Li XY, Liu JZ (2023) Exotic clasts in Chang'e-5 regolith indicative of unexplored terrane on the Moon. *Nat Astron* 7:152–159. <https://doi.org/10.1038/s41550-022-01840-7>
- Zhang AC, Hsu WB, Li XH, Ming HL, Li QL, Liu Y, Tang GQ (2011) Impact melting of lunar meteorite Dhofar 458: evidence from polycrystalline texture and decomposition of Zircon. *Meteorit Planet Sci* 46:103–115. <https://doi.org/10.1111/j.1945-5100.2010.01144.x>
- Zhang QWL, Yang M-H, Li Q-L, Liu Y, Yue Z-Y, Zhou Q, Chen L-Y, Ma H-X, Yang S-H, Tang X, Zhang G-L, Ren X, Li X-H (2024)

- Lunar farside volcanism 2.8 billion years ago from Chang'e-6 basalts. *Nature*. <https://doi.org/10.1038/s41586-024-08382-0>
- Zhou Q, Liu Y, Yang S, Li Q-L, Chen Y, Zhang G, Zhang H, Liu B, Liu D, Liu J, Wu F-Y, Li X-H, Yin Q-Z, Li C (2023) The youngest lunar Zircon reveals an extremely fractionated nature of Chang'e-5 basalt. *Geochim Cosmochim Acta* 358:126–133. <https://doi.org/10.1016/j.gca.2023.08.017>
- Zhou C, Mo B, Tang H, Gu Y, Li X, Zhu D, Yu W, Liu J (2024) Multiple sources of water preserved in impact glasses from Chang'e-5 lunar soil. *Sci Adv* 10:ead12413. <https://doi.org/10.1126/sciadv.ad12413>
- Zong K, Wang Z, Li J, He Q, Li Y, Becker H, Zhang W, Hu Z, He T, Cao K, She Z, Wu X, Xiao L, Liu Y (2022) Bulk compositions of the Chang'E-5 lunar soil: insights into chemical homogeneity, exotic addition, and origin of landing site basalts. *Geochim Cosmochim Acta* 335:284–296. <https://doi.org/10.1016/j.gca.2022.06.037>

Publisher's note Springer Nature remains neutral with regard to jurisdictional claims in published maps and institutional affiliations.